size. The third example is only related to the tilt-loss calculation. A straight section of the coalmine top entry tunnel has a top width of 2.8 m, a bottom width of 3.2 m, and a height of 3.0 m. The root-mean-square tilt angle is estimated to be 3.67°. The measured overall propagation loss for the fundamental mode was 33 dB/100 m at 900 MHz [3]. The waveguide model predicts the total propagation loss to be 38 dB/100 m if Eq. (7) for the tilt loss is used, and 64 dB/100 m if formula (A4) for the tilt loss is used. Obviously, Eq. (7) greatly enhances the accuracy of the prediction.

III. CONCLUSION

The enhancement of the well-known waveguide model for propagation loss prediction along an LOS propagation path in a tunnel is presented. The first step of the improvement was done on the tilt-loss calculation. A numerical technique to calculate the tilt loss was developed. More accurate results and larger applicable ranges were obtained. The second step was focused on the distinction of the two propagation regions in the tunnel. This was achieved by solving a novel equation. The solution of the equation yielded a distance parameter that was used to distinguish the two propagation regions. In the region before the distance point, the free-space model was used to predict the propagation loss, while in the region after the breakpoint, the waveguide model was shown to be applicable. The enhancement was demonstrated using examples. It is believed that the enhancement should be very useful for tunnel microcell design.

APPENDIX

The formulas to calculate the losses given in [2] for a rectangular tunnel are included here. The refraction loss PL_{11} in decibels over a distance d is expressed as

$$\mathrm{PL}_{11} = 4.343\lambda^2\left(\frac{\varepsilon_{r1}}{w^2\sqrt{\varepsilon_{r1}-1}} + \frac{1}{h^3\sqrt{\varepsilon_{r2}-1}}\right)d \quad \text{(A1)}$$

for horizontal polarization and as

$$\mathrm{PL}_{11} = 4.343\lambda^2\left(\frac{1}{w^3\sqrt{\varepsilon_{r1}-1}} + \frac{\varepsilon_{r2}}{h^3\sqrt{\varepsilon_{r2}-1}}\right)d \quad \text{(A2)}$$

for vertical polarization. In formulas (A1) and (A2), ε_{r1} is the relative permittivity of the rectangular tunnel sidewalls, and ε_{r2} is the relative permittivity of the rectangular tunnel floor and roof.

The roughness loss in decibels for the fundamental mode is given as

$$\mathrm{PL}_r = 4.343\pi^2 r^2\lambda\left(\frac{1}{w^4} + \frac{1}{h^4}\right)d \quad \text{(A3)}$$

where r is the root-mean-square roughness. The tilt loss in decibels for the fundamental mode is given as

$$\mathrm{PL}_t = \frac{4.343\pi^2\theta^2}{\lambda}d \quad \text{(A4)}$$

where θ is the root-mean-square tilt. The coupling loss of a half-wave dipole at (x, y) on the cross section of the tunnel can be written as

$$\mathrm{CL} = 10\log\left[0.5233\frac{\lambda^2}{wh}\cos^2\frac{\pi x}{w}\cos^2\frac{\pi y}{h}\right]. \quad \text{(A5)}$$

REFERENCES

1. S. Faruque, Cellular mobile systems engineering, Artech House, Boston, MA, 1996.
2. A.G. Emslie, R.L. Lagace, and P.F. Strong, Theory of the propagation of UHF radio waves in coal mine tunnels, IEEE Trans Antennas Propagat AP-23 (1975), 192–205.
3. G.X. Zheng, J.H. Sheng, and Y.P. Zhang, Propagation of UHF radio waves in trapezoidal tunnels, Microwave Opt Technol Lett 20 (1999), 295–297.

A NEW APPROACH TO THE ORCHARD–ELLIOTT PATTERN SYNTHESIS ALGORITHM USING LMS AND PSEUDOINVERSE TECHNIQUES

R. Shavit[1] and S. Levy[1]
[1] Department of Electrical and Computer Engineering
Ben-Gurion University of the Negev
Beer-Sheva 84105, Israel

Received 10 January 2001

ABSTRACT: *A new approach to the Orchard–Elliott pattern synthesis algorithm based on the least mean-square (LMS) technique and the pseudoinverse technique is described. The new algorithm offers better initial conditions and avoids possible divergence problems throughout the iteration process. The array current distribution obtained is optimized using a genetic algorithm. The effectiveness of the new approach is demonstrated on a linear array with a symmetric flat-topped radiation pattern.* © 2001 John Wiley & Sons, Inc. Microwave Opt Technol Lett 30: 12–15, 2001.

Key words: *array synthesis algorithms*

I. INTRODUCTION

The growing interest in wireless communication and the commercialization of phased-array applications with a limited field of view increased the efforts to explore new techniques for shaped radiation-pattern synthesis. The shaped beams are used for frequency and polarization reuse in a multicell angular sector, as well as to avoid interferences. Several techniques for the array pattern synthesis are available: Fourier series synthesis [1], the Woodward–Lawson method [2], and the Orchard–Elliott technique [3]. By far, the Orchard–Elliott technique is the most effective for shaped-beam synthesis. In contrast to the other techniques, the Orchard–Elliott technique synthesizes the power pattern instead of the field pattern to increase the degrees of freedom in the design process.

The Orchard–Elliott technique is a procedure based on first-order linearization of the array pattern. The pattern is expressed in a polynomial representation form with N-1 roots (N being the array elements number). The initial roots are uniformly distributed on the Schelkunoff circle [4]. Lineariza-

tion of the error between the desired and calculated radiation pattern results in a square matrix equation. The change in the roots location in each iteration is determined by the solution of the matrix equation. Occasionally, the inverted square matrix becomes singular (nonsquare). By the end of the iterative procedure, the algorithm offers 2^{N1} different current distributions ($N1$ being the number of roots in the shaped region), yielding the same radiation pattern. The most practical current distribution is chosen from this ensemble.

II. THE NEW APPROACH

The radiation pattern of a linear array oriented along the z-axis can be written in the form

$$F(\theta) = \sum_{n=1}^{N} I_n e^{jnkd\cos\theta}$$

in which I_n denotes the current distribution and d is the element spacing. If $F(\theta)$ is sampled at M discrete angles $(\theta_1, \ldots, \theta_M)$, this radiation pattern can be rewritten in the following matrix form

$$\begin{bmatrix} F(\theta_1) \\ F(\theta_2) \\ \vdots \\ F(\theta_M) \end{bmatrix} = [I_1 \cdots I_N] \begin{bmatrix} e^{jkd\cos\theta_1} & \cdots & e^{jkd\cos\theta_M} \\ \cdot & \cdots & \cdot \\ \cdot & \cdots & \cdot \\ \cdot & \cdots & \cdot \\ e^{jNkd\cos\theta_1} & \cdots & e^{jNkd\cos\theta_M} \end{bmatrix} \tag{1}$$

or, in short-form notation, $[F] = [I][E]$. The error between the desired radiation pattern $D(\theta)$ and the computed radiation pattern $F(\theta)$ can be minimized using the LMS technique [5]. The result is the current distribution for the minimum error $[I] = [D][E]^T([E][E]^T)^{-1}$ (T denotes transpose). This result can be used as the initial current distribution to the Orchard–Elliott iterative algorithm. Figure 1 shows a comparison between the initial radiation pattern for an 80-element linear array ($\lambda/2$ spacing) obtained with the new approach compared to the initial radiation pattern obtained with the original algorithm. The desired flat-topped radiation pattern beamwidth is 70°, and the ripple in the shaped region is ± 0.25 dB. In the unshaped region, the requested sidelobe level is -40 dB. One can observe a better starting pattern than the pattern obtained with uniform roots distribution as suggested in the Orchard–Elliott algorithm. The Orchard–Elliott iterative procedure starts with the array power pattern given in the form

$$\hat{g} = |F|^2 = \prod_{n=1}^{N} (1 - 2e^{a_n}\cos(\phi - b_n) + e^{2a_n}) \tag{2}$$

where $\phi = kd\sin\theta$ and $w_n = \exp(a_n + jb_n)$ are the roots in the w complex plane. If Eq. (2) is evaluated at extreme angles (minima and maxima in the shaped region and maxima in the unshaped region), it can be approximated by first-order linearization and transformed into a matrix equation:

$$A\Delta x = g - \hat{g} \tag{3}$$

in which $g - \hat{g}$ is the error between the desired g and calculated $\hat{g}$ power patterns. A is a matrix, which contains derivatives of the power pattern with respect to the variables a_n and b_n (evaluated at the same angles), and Δx is the required increment of the variables a_n, b_n for the next iterative step. At each iteration, the roots change their location. Occasionally, the number of roots in the shaped region is not preserved, and the matrix A becomes nonsquare. In the original Orchard–Elliott algorithm, this problem is avoided by allowing flexible boundaries to the shaped region throughout the iteration process, such that the matrix A is always kept square even if the roots of the shaped region move outside it. In the proposed approach, there is no need to allow these flexible boundaries, and if the matrix A becomes nonsquare it is possible to obtain a solution using the pseudoinverse technique [5]. This approach results in a variation of Eq. (3):

$$\Delta x = (A^T A)^{-1} A^T (g - \hat{g}). \tag{4}$$

Figure 2 shows two examples of a flat-topped shaped radiation pattern with -40 dB sidelobe level in which the matrix

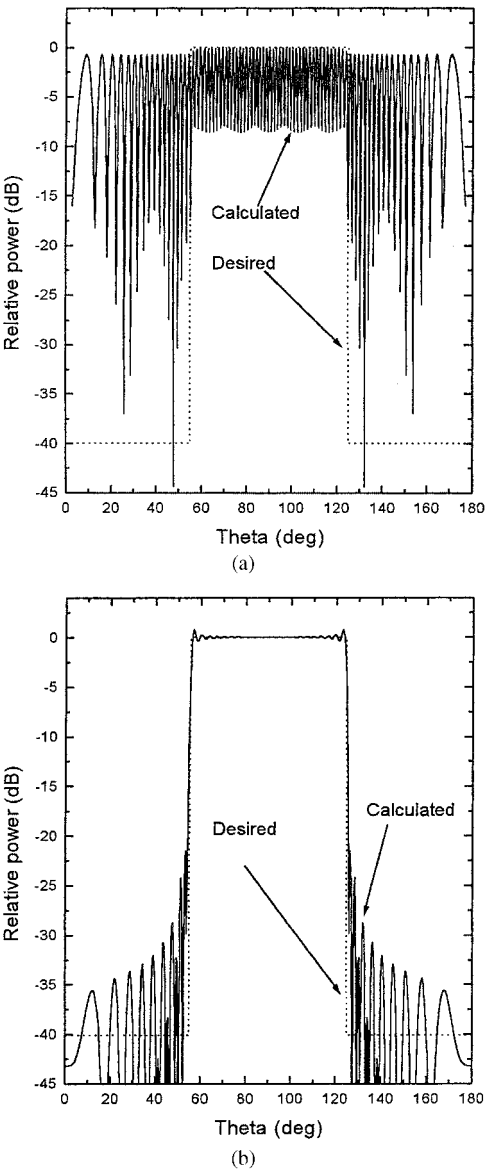

Figure 1 Initial radiation pattern of an 80-element linear array, $\lambda/2$ spacing (a) for uniform root distribution as suggested in Orchard–Elliott algorithm, (b) for root distribution obtained with the LMS technique

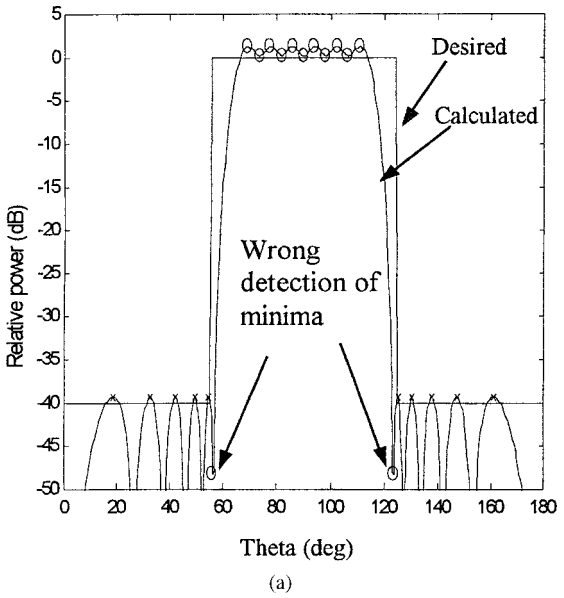

Figure 2 Two examples of a flat-topped shaped radiation pattern in which the matrix A becomes singular. (a) Minima from unshaped region penetrates in the shaped region. (b) A deflection point is obtained, avoiding detection of a minima and maxima in the shaped region

A becomes singular if the shaped region boundaries are strictly kept. In (a), one can observe that a minima of a sidelobe from the unshaped region penetrates into the shaped region, and in (b), a deflection point is generated throughout the iteration process, avoiding detection of a minima and maxima in the shaped region. These cases can be treated without any problem by the new approach since there is no mandatory requirement that the matrix A be square.

Once the algorithm converges, a genetic algorithm [6] is applied to obtain the optimal current distribution from the 2^{N1} different current distributions obtained. The cost function for the optimization is a penalizing high excitation ratio of adjacent element currents I_n/I_{n+1}.

III. NUMERICAL ANALYSIS

As an example, we considered a flat-topped radiation pattern generated by a 16-element linear array with $\lambda/2$ spacing. In the shaped region, the beamwidth was 70° with a ripple of ± 0.1 dB. In the unshaped region, the sidelobe level was -30 dB. Figure 3 shows the radiation pattern and the optimum current distribution obtained with the proposed algorithm and the genetic algorithm with a population of 100, mutation 20%, and ten iterations. One can observe a good convergence to the desired pattern and the current distribution.

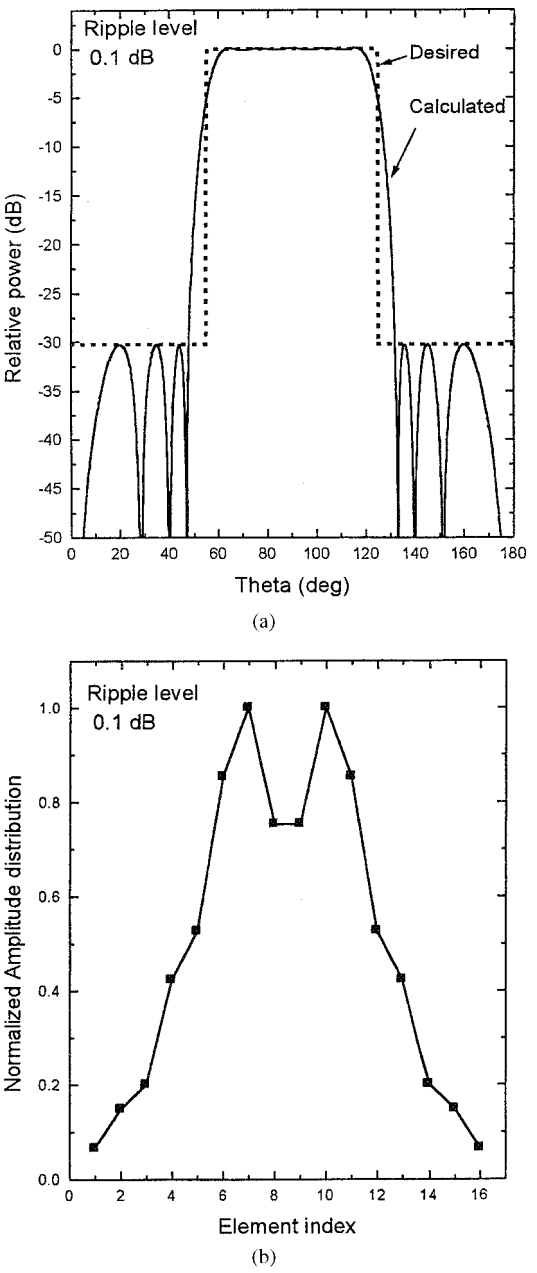

Figure 3 Numerical results for a flat-topped radiation pattern generated by a 16-element linear array, $\lambda/2$ spacing. (a) Radiation pattern. (b) Current distribution

IV. CONCLUSIONS

A new approach to the Orchard–Elliott algorithm for the synthesis of shaped radiation patterns was presented. The synthesis uses the LMS technique to obtain a better initial root distribution for the first iteration, and the pseudoinverse technique to avoid possible divergence throughout the iteration process. The effectiveness of the new approach was

demonstrated on a linear array with a symmetric flat-topped radiation pattern.

ACKNOWLEDGMENT

The authors would like to thank Prof. Francisco Ares-Pena from the University of Santiago at Compostela, Spain, for fruitful discussions on the subject, and for providing computer results of synthesized shaped radiation patterns based on the original Orchard–Elliott algorithm.

REFERENCES

1. R.J. Mailloux, Phased array antenna handbook, Artech House, Boston, MA, London, England, 1993.
2. P.M. Woodward and J.P. Lawson, The theoretical precision with which an arbitrary radiation pattern may be obtained from a source of finite size, Proc IEEE 36 (1948), 120–126.
3. H.J. Orchard, R.S. Elliott, and G.J. Stern, Optimising the synthesis of shaped antenna patterns, Proc Inst Elect Eng 132 (1985), 63–68.
4. R.S. Elliott, Antenna theory and design, Prentice-Hall, Englewood Cliffs, NJ, 1981.
5. M.R. Hestenes, Pseudo-inverse and conjugate gradients, Commun ACM 18 (1975), 40–43.
6. Y. Rahmat-Samii and E. Michielssen, Electromagnetic optimization by genetic algorithms, Wiley, New York, 1999.

TRANSMISSION LINE – PERIODIC CIRCUIT REPRESENTATION OF PLANAR MICROWAVE PHOTONIC BANDGAP STRUCTURES

M. Rahman[1] and M. A. Stuchly[1]
[1] Department of Electrical and Computer Engineering
University of Victoria
Victoria, B.C. V8W 3P6, Canada

Received 18 January 2001

ABSTRACT: *Planar photonic bandgap structures have been modeled using the theory of transmission lines and periodic circuits. The method allows for fast and accurate computation of the dispersion diagram, and thus prediction of the stopbands for two directions of propagation. Results obtained by the proposed analytic method are in agreement with previously published numerical data for two structures. Additional numerical evaluations of the reflection phase with the finite-difference time-domain (FDTD) method confirm the validity of the analytic model within the limits of its applicability. They also further confirm previous observations that wave propagation in directions other than two principal axes results in a narrower stopband.* © 2001 John Wiley & Sons, Inc. Microwave Opt Technol Lett 30: 15–19, 2001.

Key words: *periodic structure; microstrip line; PBG structure; FDTD*

I. INTRODUCTION

Photonic bandgap structures (PBGs) are composite periodic structures that exhibit transmission (pass) and reflection (stop) bands in their frequency response [1]. They can be made of dielectric only [2] or of metallic elements embedded in a dielectric material [3]. Two- or three-dimensional arrangements of the PBG crystals have been explored [4]. Numerous engineering applications of these structures have been described at microwave frequencies, such as microstrip filters [5], high-power components [6], magnetic conducting surfaces [7], and substrates for printed antennas [8–10]. These structures are typically analyzed numerically by calculating the dispersion diagram ($\beta - \omega$) [11, 12], the transmission and reflection coefficients [13, 14], and the reflection phase [7].

Recently, 2-D PBG structures that are finite in the third dimension have been proposed at microwave frequencies [15, 16]. These structures suppress the surface currents, and serve as high-impedance surfaces within the stopband. The PBG structures presented in [15] and [16] have been analyzed numerically. The surface in [15] has also been modeled using an effective medium model with lumped inductance L and capacitance C that can only predict the first resonant frequency, but not the bandgaps.

In this paper, we explore an analytical model for 2-D microwave PBG structures, such as those in [15] and [16]. The impedance of each section of the structures is calculated using transmission-line theory. The whole structure is then analyzed using the theory of periodic circuits [17]. Results from this analytic model are compared with previously published numerical data. The phase of the reflection coefficient of a wave normally incident on the structures computed with a finite-difference time-domain (FDTD) method is also compared.

II. ANALYTICAL MODEL

Figure 1 shows schematic diagrams of the two high-impedance surfaces modeled. The lattice in Figure 1(a) consists of square metal sheets connected to the continuous ground plane through thin wires, as in [15], and the lattice in Figure 1(b) consists of square metal patches with four narrow connecting branches placed over a ground plane, as in [16]. These circuits can be considered as arrays of reactively loaded resonators coupled by gap capacitors. Each unit cell of the structures is a half-wavelength microstrip resonator ($f \approx (c/2w\sqrt{\varepsilon_{\text{eff}}})$ if the shorting post [Fig. 1(a)] and connecting branches [Fig. 1(b)] are disregarded. However, an additional resonant frequency below the half-wavelength resonance results from the reactive loading of microstrip resonators [18]. Shorting pins [19] or narrow connecting branches [20] can provide load reactance. At the resonant frequency, the structure radiates energy into the space above, but a small amount of the energy also propagates along the structure. Thus, the surfaces shown in Figure 1(a) and (b) can be considered as structures periodically loaded with gap capacitances and reactances provided by the shorting pins [Fig. 1(a)] or connecting branches [Fig. 1(b)].

Both the TE and TM modes with respect to the normal to the surface exist in these structures (also called LSE and LSM modes). The TE and TM modes are coupled, and neither mode can exist by itself [21]. Each reactively loaded resonator of Figure 1(a) and (b) can be represented by an equivalent circuit shown in Figure 1(c), where Z_p is the reactance of the resonator. The capacitive reactance X_c represents the coupling capacitor between the neighboring resonators. These are the two contributions to the total impedance between the two nodes of the periodic circuits shown in Figure 2 for the wave propagation in the x-direction. The centrally located shorting pin in Figure 1(a) provides the inductive loading X_l of the resonator, with induc-

Contract grant sponsor: Commonwealth Scholarship
Contract grant sponsor: NSERC Industrial Research Chair